Enriched Representation Learning for Longitudinal Chest X-ray Analysis: A Novel Approach for Improved Disease Detection and Localization

Xiangyu Li¹, Armand Ovanessians², and Hua Wang¹

¹Department of Computer Science

²Department of Quantitative Biosciences and Engineering

Colorado School of Mines, Golden, Colorado, USA

Email: {lixiangyu, ovanessians}@mines.edu, huawangcs@gmail.com

Abstract-Chest X-rays are commonly used for diagnosing and characterizing lung diseases, but the complex morphological patterns in radiographic appearances can challenge clinicians in making accurate diagnoses. To address this challenge, various learning methods have been developed for algorithm-aided disease detection and automated diagnosis. However, most existing methods fail to account for the heterogeneous variability in longitudinal imaging records and the presence of missing or inconsistent temporal data. In this paper, we propose a novel longitudinal learning framework that enriches inconsistent imaging data over sequential time points by leveraging twodimensional principal component analysis and a robust adaptive loss function. We also derive an efficient solution algorithm that ensures both objective and sequence convergence for the nonconvex optimization problem. Our experiments on the CheXpert dataset demonstrate improved performance in capturing indicative abnormalities in medical images and achieving satisfactory diagnoses. We believe that our method will be of significant interest to the research community working on medical image analysis.

Index Terms—Longitudinal Learning, Representation Enrichment, Robust Learning.

I. INTRODUCTION

Chest X-rays are essential for clinical practice and medical research, providing valuable insights into structural abnormalities, pulmonary disease classification, disease progression tracking, and potential diagnoses [1], [2]. However, accurate diagnosis faces significant challenges. Firstly, many patients exhibit multiple pulmonary or cardiological diseases, and different patients may share similar clinical phenotypes and radiographic appearances [2], [18], [27], resulting in complex morphological patterns and distributions in chest images. Secondly, current diagnostic processes heavily rely on the expertise and experience of radiologists or physicians, making it difficult to achieve consensus on imaging findings when physicians have varying interpretations.

To address these challenges, numerous machine learning methods have been developed for algorithm-aided detection and automated diagnosis [6], [17], [19], [20]. However, most of these methods fail to adequately account for variations in longitudinal imaging records. Longitudinal data, which comprises repeated measurements over time for individual

patients, is crucial for studying disease progression in patients with long treatment courses. However, analyzing longitudinal variations on an individual level poses a notable challenge due to missing or inconsistent records [5], [9]. Traditional matrix/tensor completion methods, employing sparse learning or deep neural networks [3], [29], often fail to effectively address the problem of missing or inconsistent data and may even discard available images [4].

In this paper, we propose a novel approach to tackle the aforementioned challenges. Our method aims to learn a pair of projections (L and R) and utilize them to project the image from the last visit into an enriched form. By employing Two-Dimensional (2D) Principal Component Analysis (PCA) to learn these projections, our method can naturally handle temporal image sequences with varying numbers of images, even when the time points for capturing images are not aligned, as illustrated in Fig. 1. Moreover, our method effectively handles irregular missing images in temporal medical data, where the imaging time points for a patient are generally misaligned with those of other patients. This is crucial because images taken at different time points can potentially act as outliers when training a learning method for other patients. To address this issue, we integrate an adaptive loss in our 2D PCA objective function.

Our proposed method offers several major contributions. Firstly, we derive an efficient solution algorithm with guaranteed objective convergence and sequence convergence, providing a solid mathematical foundation for our approach. Unlike existing papers that use the alternating optimization method, which only ensures a decrease in the objective value but not algorithm convergence, our method guarantees convergence. Secondly, our method achieves high prediction accuracy while maintaining an efficient training process, in contrast to deep learning methods that often come with high computational costs and lengthy training times. Additionally, our method requires tuning only four hyperparameters, significantly reducing the complexity compared to deep learning methods.

We conduct a series of experiments on the CheXpert dataset [11], [16], [26], which consists of 224,316 chest X-ray scans from 65,240 patients. While this dataset has gained

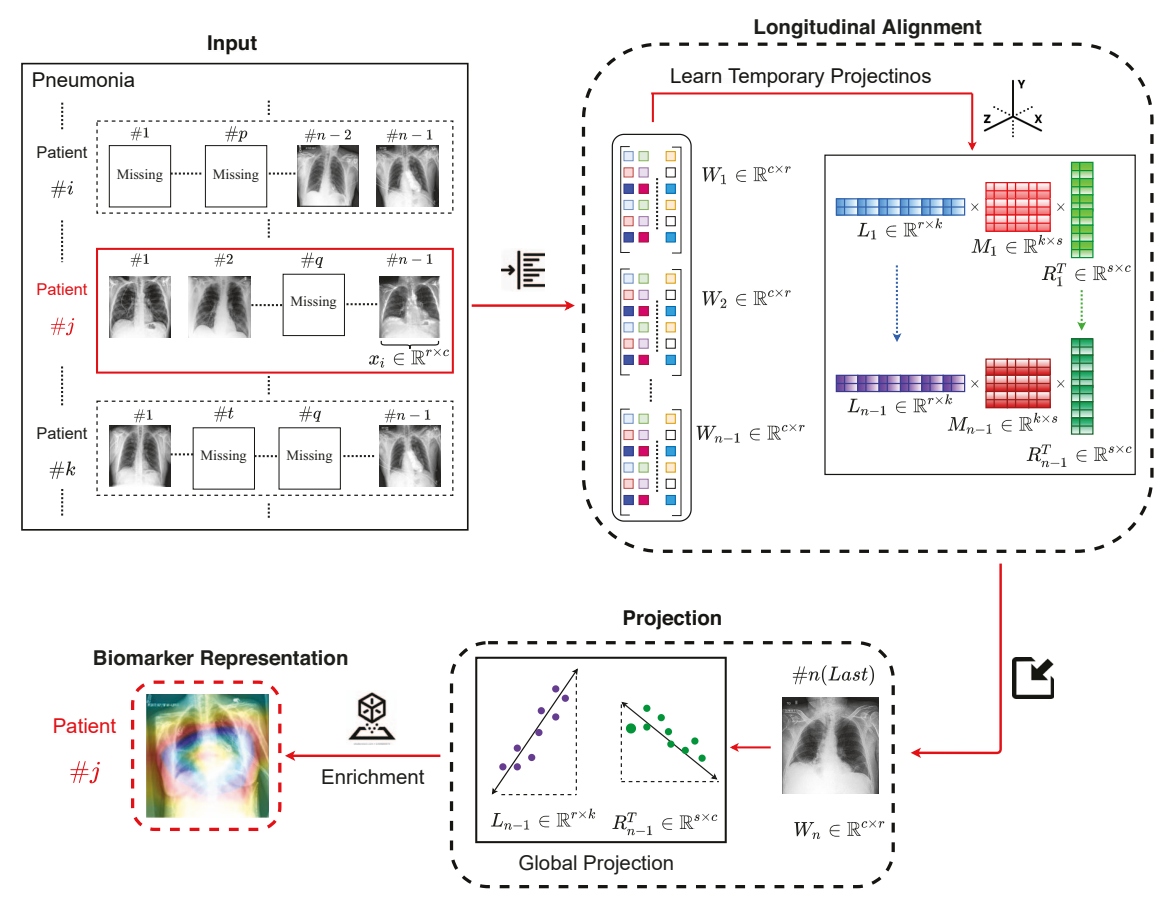


Fig. 1. The illustration of the proposed longitudinal embedding method representation for the CheXpert Database. Patient j with pneumonia is used as an example, with a medical history comprising a total of n chest images and one missing record (image q). The images from 1 to n-1 are aligned to create the baseline samples. By learning from these baseline samples, we sequentially obtain and update two temporary projections. The final learned projections, called global projections, integrate all past medical features. In the last step, we project the last scanned image (n) onto the global projections to obtain a 2-D enriched phenotypic representation.

widespread recognition, most research works utilizing it are limited by the aforementioned problems. In our study, we focus on pulmonary diseases such as pneumonia, pneumothorax, edema, lung lesion, and lung opacity. The experimental findings demonstrate enhanced automated diagnosis accuracy and greater interpretability of our method.

In summary, our proposed longitudinal embedding method provides a novel approach to leveraging temporal information in medical image analysis. By addressing the challenges of multiple diseases and varying longitudinal records, our method offers improved diagnostic accuracy and interpretability. The mathematical foundation, efficient training process, and promising experimental results highlight the potential impact of our approach in the field of algorithm-aided diagnosis for chest X-rays.

II. OBJECTIVE AND SOLUTION ALGORITHM

In this section, we present the novel objective and solution algorithm of our approach. We build upon the methodology of 2D-PCA and the adaptive loss function, which serve as the foundation of our method. Subsequently, we introduce our robust longitudinal embedding method, highlighting the design choices that differentiate our approach. Given the non-convex nature of our objective function, we propose a novel alternating minimization algorithm as an effective optimization technique. This algorithm provides closed-form solutions for our objective function, surpassing the performance of other optimization methods. Through rigorous mathematical analysis, we demonstrate that both the objective and solution converge to a global optimum at a sub-linear rate. Our proposed methodology offers a novel and effective approach for longitudinal medical image analysis, showcasing our contributions to the field.

A. Objective Function

The objective of 2D-PCA [7] is to decompose a set of 2D maps $\{A_i\}_{i=1}^n$, where each $A_i \in \mathbb{R}^{r \times c}$, into a linear combination of orthogonal 2D bases. The objective function is formulated as follows:

$$\min_{L \in \mathbb{R}^{r \times p}, R \in \mathbb{R}^{c \times s}, M_i \in \mathbb{R}^{p \times s}} J = h(L, M_i, R)$$

$$= \sum_{i=1}^{n} ||A_i - LM_i R^T||_F^2, \tag{1}$$

subject to the constraints $L^TL=I_p$ and $R^TR=I_s$. Here, $L=\tilde{U}_p=(\tilde{u_1},\ldots,\tilde{u_p}),\ R=\tilde{V}_s=(\tilde{v_1},\ldots,\tilde{v_s}),$ and $M_i=\tilde{U}_p^TA_iV_s$.

However, the squared Frobenius norm loss function used in this objective function is sensitive to noise or corrupted observations, making the learning performance vulnerable to outliers. To overcome this limitation, we propose to use the novel adaptive loss function prposed in [25] that combines the ℓ_1 -norm and ℓ_2 -norm distances, thereby enhancing robustness against outliers. The adaptive loss function is defined as follows:

$$||X||_{\sigma} = (1+\sigma) \sum_{i} \frac{(1+\sigma)||x^{i}||_{2}}{||x^{i}||_{2} + \sigma},$$
 (2)

where σ is an adaptive parameter and x^i represents the i-th row of matrix X. This novel loss function is grounded on the assumption that most data points yield small losses, following a Gaussian distribution, while only a few data points exhibit large losses, following a Laplacian distribution.

Motivated by these findings, we incorporate the adaptive loss function defined in Eq. (2) into the objective function in Eq. (1), enabling robustness against outliers in longitudinal imaging datasets. Thus, our proposed objective function becomes:

$$h(L, M_i, R) = \sum_{L \in \mathbb{R}^{r \times k}, R \in \mathbb{R}^{c \times s}, M_i \in \mathbb{R}^{k \times s}} = \sum_{i=1}^n ||A_i - LM_i R^T||_{\sigma},$$

$$s.t. \ L^T L = I_k, \ R^T R = I_s,$$
(3)

where σ is the adaptive parameter and $\{A_i \in \mathbb{R}^{r \times s}\}_{i=1}^n$ represents a set of input lung images for the study.

While the motivation behind the new objective in Eq. (3) is sound, finding its closed-form solution poses a significant challenge due to the non-convex nature of the matrix factorization problem [25]. To tackle this challenge, we propose a novel alternately updating method, which transforms the objective function into a convex form. This method updates the objective alternately with respect to one parameter while keeping the others fixed at each time step. The updating procedure can be summarized as follows:

$$L_{k+1} = \sum_{i=1}^{n} ||A_i - L\{M_i\}_k R_k^T||_{\sigma},$$

$$\{M_i\}_{k+1} = \sum_{i=1}^{n} ||A_i - L_k M_i R_k^T||_{\sigma},$$

$$R_{k+1} = \sum_{i=1}^{n} ||A_i - L_k \{M_i\}_k R^T||_{\sigma}.$$
(4)

B. Proposed Algorithm

In this section, we describe the procedures for updating the algorithm at each time step. We derive closed-form solutions for L, $\{M_i\}$, and R are as follows:

For L_{k+1} , we have:

$$L_{k+1} = \underset{L^T L = I}{\arg \max} \sum_{i=1}^{n} Tr(L^T E) = Y Z^T,$$
 (5)

where Y and Z are obtained from $[Y, \Sigma, Z] = \text{svd}(E)$ [29]. Here, E is given by:

$$E = 2d_i(L_k\{M_i\}_k R_k^T - A_i)R_k\{M_i\}_k^T + \mu L_k,$$

and $d_i=(1+\sigma)\frac{||A_i-L\{M_i\}R^T||_F+2\sigma}{2(||A_i-L\{M_i\}R^T||_F+\sigma)^2}$ is a weighting factor derived from the adaptive loss function [25].

For $\{M_i\}_{k+1}$, we have:

$$\{M_i\}_{k+1} = \arg\max \sum_{i=1}^{n} Tr(\{M_i\}^T G) = PQ^T,$$
 (6)

where $G=2d_iL_k^T(L_k\{M_i\}_kR_k^T-A_i)R_k+\omega\{M_i\}_k$, and $[P,\Sigma,Q]=\operatorname{svd}(G)$.

For R_{k+1} , we have:

$$R_{k+1} = \underset{R^T}{\arg\max} \sum_{i=1}^{n} Tr(R^T F) = HJ^T,$$
 (7)

where $F = 2d_i(R_k\{M_i\}_k^T L_k^T - A_i^T)L_k\{M_i\}_k + \lambda R_k$, and $[H, \Sigma, J] = \text{svd}(F)$.

Our proposed algorithm, which efficiently updates the variables at each iteration, is summarized in Algorithm 1.

Algorithm 1 Alternating Linearized Minimization

Require: Data $A_i \in \mathbb{R}^{r \times c}$, rank of factors k, regularization parameters λ , ω , and μ , and number of iterations I.

- 1: Initialization: $L_0 \in \mathbb{R}^{r \times k}, \{M_i\}_0 \in \mathbb{R}^{k \times s}, \text{ and } R_0 \in \mathbb{R}^{e \times s}$
- 2: while $k \leq K$ do
- 3: Optimize L_{k+1} as in Eq. (5).
- 4: Optimize $\{M_i\}_{k+1}$ as in Eq. (6).
- 5: Optimize R_{k+1} as in Eq. (7).
- 6: $k \leftarrow k + 1$.
- 7: end while
- 8: **Output:** $(L, R, \{M_i\}_{k=1}^n)$.

The complexity analysis and convergence analysis of the algorithm are not provided here due to space limit and will be provided in the extended journal version of this paper.

Following [23], [24], we learn the enriched image representations as follows. Once L and R are learned from a sequence of X-ray images from the earlier medical records, they are used to project the X-ray image from the most recent visit and the projected representation is used for subsequent diagnosis.

III. EXPERIMENTAL EVALUATION

In this section, we present a detailed evaluation of our proposed method and discuss its superior performance compared to existing approaches. We conducted experiments on the CheXpert dataset [27], which consists of 224,316 chest radiographs from 65,240 patients. The dataset includes various pulmonary diseases, but our study primarily focuses on the first five lung diseases: pneumonia, pneumothorax, edema, lung lesion, and lung opacity.

A. Convergence Analysis

We first evaluate the convergence behavior of our method on the pneumonia dataset. Figure 2 shows the convergence performance of the solution sequence $L,\,M,\,$ and R in our objective function. It can be observed that both L and R exhibit fluctuations at the early steps, followed by a moderate decrease. Beyond time step 200, both curves decline rapidly and eventually converge to a constant value. The variable M decreases significantly in the initial stages and then moves towards the converging point with slight oscillations. These results align with our mathematical analysis, confirming the low computational cost of our method.

B. Gender Analysis

Gender differences are often assumed to exist among patients with pulmonary diseases in terms of susceptibility, severity, and disease progression, mainly attributed to the higher prevalence of smoking among men [12]. However, recent research suggests that the gender difference may not be as significant as previously thought, as these diseases are also commonly seen in women. To investigate the gender effect in the learning process, we divided all patients into two groups: male and female. We used the Densenet-121 CNN method [15] as the classifier for both enriched representations and original images. Table I shows the detection accuracy (Acc score) and Table II shows F1 scores of our approach on male and female patients, and we compare our results to several state-of-the-art methods, including longitudinal-based methods such as Distance-LSTM [10] and Ori-CNN [22], as well as projection-based methods such as 2D-PCA [7], R1-PCA [8], L1-2DPCA [21], Stacked AutoEncoder (AE) [28], Locality Preserving Projections (LPP) [13], and Restricted Boltzmann Machine (RBM) [14].

We observe that our approach outperforms other methods with significant margins. Furthermore, the detection accuracy in the male group is slightly higher than that of the female group for patients with the diseases of pneumonia, edema, lung lesion, or lung opacity. This could be attributed to the longstanding pathological manifestation of some male smokers who usually have a longer smoking history compared to female patients. However, due to the increasing prevalence of smoking in females in recent years, other factors such as exposure to second-hand smoke, air pollution, or hormonal effects have made female patients susceptible to pulmonary diseases. In this scenario, our 2D enriched imaging representation is capable of embedding all important features along the time points into a single image. Moreover, this enriched representation can provide physicians with comprehensive insights into the underlying mechanism for different patients.

IV. CONCLUSION

In conclusion, we have proposed a novel longitudinal embedding method that enhances the effectiveness of noninvasive diagnostic determination and facilitates clinical practice. Our method enables machine learning algorithms to make reliable diagnoses using varying numbers of samples, while

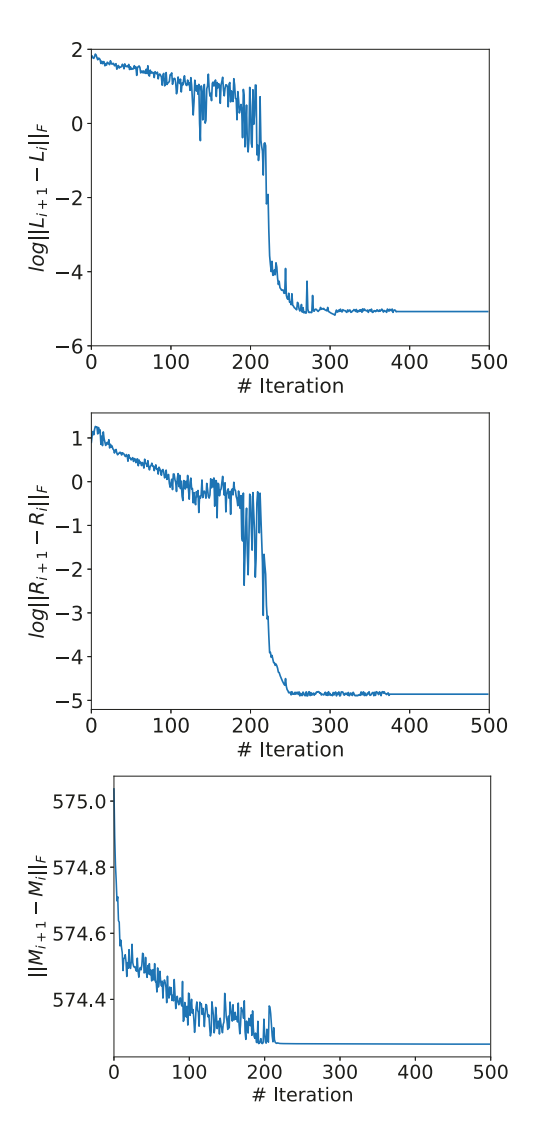


Fig. 2. Convergence behavior of the solution sequence L, M, and R in our objective function. **Left**: Convergence of L with respect to the Frobenius norm, $\log ||L_{i+1} - L_i||_F$, indicating the convergence rate of the left projection. **Right**: Convergence of M with respect to the Frobenius norm, $\log ||M_{i+1} - M_i||_F$, demonstrating the convergence rate of the enriched representation. **Middle**: Convergence of R with respect to the Frobenius norm, $\log ||R_{i+1} - R_i||_F$, illustrating the convergence rate of the right projection.

also reducing the storage volume of large and computationintensive real-world medical datasets. The experiments conducted on the CheXpert dataset have successfully validated our mathematical analysis and demonstrated the advantages of enriched representations over original images in identifying and localizing abnormalities.

The longitudinal embedding approach captures temporal information by combining multiple imaging records into a single enriched representation. This representation provides a comprehensive view of the patient's condition, allowing for more accurate and interpretable diagnostic outcomes. Our method has shown superior performance compared to state-

TABLE I

THE CLASSIFICATION PERFORMANCE OF THE LONGITUDINAL EMBEDDING AND ORIGINAL IMAGES WITH RESPECT TO GENDER DISTRIBUTION.

SPECIFICALLY, WE COMPARED THE CLASSIFICATION RESULTS OF THE EMBEDDINGS AND THE ORIGINAL IMAGES USING THE ACCURACY SCORE (ACC)

METRIC.

ACC Score	Gender	Ours	Dis-LSTM [10]	Ori-CNN [22]	2D-PCA [7]	R1-PCA [8]
Pneumonia	Male Female	$\begin{array}{c} 0.844 \pm 0.029 \\ 0.835 \pm 0.028 \end{array}$	$\begin{array}{c} 0.831 \pm 0.032 \\ 0.821 \pm 0.031 \end{array}$	$\begin{array}{c} 0.830 \pm 0.031 \\ 0.813 \pm 0.029 \end{array}$	$\begin{array}{c} 0.795 \pm 0.034 \\ 0.781 \pm 0.033 \end{array}$	$\begin{array}{c} 0.810 \pm 0.030 \\ 0.801 \pm 0.029 \end{array}$
Pneumothorax	Male Female	$\begin{array}{c} 0.837 \pm 0.030 \\ 0.830 \pm 0.029 \end{array}$	$\begin{array}{c} 0.824 \pm 0.033 \\ 0.811 \pm 0.032 \end{array}$	$\begin{array}{c} 0.825 \pm 0.032 \\ 0.813 \pm 0.030 \end{array}$	$\begin{array}{c} 0.809 \pm 0.035 \\ 0.803 \pm 0.034 \end{array}$	$\begin{array}{c} 0.812\pm0.031 \\ 0.810\pm0.030 \end{array}$
Edema	Male Female	$\begin{array}{c} 0.832 \pm 0.031 \\ 0.825 \pm 0.030 \end{array}$	$\begin{array}{c} 0.817 \pm 0.034 \\ 0.813 \pm 0.033 \end{array}$	$\begin{array}{c} 0.820\pm0.033 \\ 0.813\pm0.031 \end{array}$	$\begin{array}{c} 0.796 \pm 0.036 \\ 0.792 \pm 0.035 \end{array}$	0.804 ± 0.032 0.800 ± 0.031
Lung Lesion	Male Female	0.815 ± 0.032 0.807 ± 0.031	0.800 ± 0.035 0.787 ± 0.034	0.799 ± 0.034 0.787 ± 0.032	0.781 ± 0.037 0.774 ± 0.036	$\begin{array}{c} 0.795 \pm 0.033 \\ 0.782 \pm 0.032 \end{array}$
Lung Opacity	Male Female	0.841 ± 0.033 0.821 ± 0.032	0.822 ± 0.036 0.811 ± 0.035	0.822 ± 0.035 0.810 ± 0.033	0.806 ± 0.038 0.798 ± 0.037	$\begin{array}{c} 0.813 \pm 0.034 \\ 0.808 \pm 0.033 \end{array}$
ACC Score	Gender	L1-2DPCA [21]	AE [28]	LPP [13]	RBM [14]	Original
Pneumonia	Male Female	$\begin{array}{c} 0.815 \pm 0.026 \\ 0.799 \pm 0.025 \end{array}$	$\begin{array}{c} 0.822\pm0.033 \\ 0.820\pm0.032 \end{array}$	$\begin{array}{c} 0.818 \pm 0.028 \\ 0.803 \pm 0.027 \end{array}$	0.797 ± 0.032 0.784 ± 0.031	$\begin{array}{c} 0.787 \pm 0.027 \\ 0.772 \pm 0.026 \end{array}$
Pneumothorax	Male Female	$\begin{array}{c} 0.784 \pm 0.027 \\ 0.790 \pm 0.026 \end{array}$	0.813 ± 0.034 0.801 ± 0.033	0.806 ± 0.029 0.792 ± 0.028	0.806 ± 0.034 0.789 ± 0.033	$\begin{array}{c} 0.779 \pm 0.028 \\ 0.782 \pm 0.027 \end{array}$
Edema	Male Female	0.793 ± 0.028 0.774 ± 0.027	0.813 ± 0.035 0.807 ± 0.034	0.809 ± 0.030 0.799 ± 0.029	0.814 ± 0.035 0.812 ± 0.034	$\begin{array}{c} 0.770 \pm 0.029 \\ 0.766 \pm 0.028 \end{array}$
Lung Lesion	Male Female	0.797 ± 0.029 0.773 ± 0.028	0.799 ± 0.036 0.784 ± 0.035	0.786 ± 0.031 0.773 ± 0.030	0.781 ± 0.036 0.770 ± 0.035	$\begin{array}{c} 0.772 \pm 0.030 \\ 0.769 \pm 0.029 \end{array}$
Lung Opacity	Male Female	0.793 ± 0.030 0.797 ± 0.029	$\begin{array}{c} 0.812 \pm 0.037 \\ 0.809 \pm 0.036 \end{array}$	$\begin{array}{c} 0.808 \pm 0.032 \\ 0.792 \pm 0.031 \end{array}$	0.786 ± 0.037 0.780 ± 0.036	$\begin{array}{c} 0.775 \pm 0.031 \\ 0.771 \pm 0.030 \end{array}$

of-the-art techniques, achieving higher accuracy in detecting pulmonary diseases across different gender distributions.

Furthermore, we have investigated the effect of treatment time on the accuracy of our method, revealing the importance of considering individual treatment courses for patients with pulmonary abnormalities. By understanding the optimal treatment duration for different diseases, our method can assist physicians in determining appropriate treatment plans and monitoring disease progression.

The interpretability of our enriched representations has been demonstrated through visualizations that highlight the most indicative areas within the images. These visualizations aid in clinical diagnosis by providing insights into pathological patterns and facilitating the identification of relevant abnormalities.

Overall, our longitudinal embedding method offers a valuable tool for non-invasive diagnostics in the field of medical imaging. By leveraging temporal information and reducing the computational burden, our approach has the potential to improve healthcare outcomes and enhance the efficiency of medical decision-making processes. Future research can explore the application of our method to other medical domains and investigate its effectiveness in longitudinal studies and personalized medicine.

ACKNOWLEDGMENT

Corresponding author: Hua Wang (huawangcs@gmail.com).

This work was supported in part by the National Science Foundation (NSF) under the grants of IIS 1652943, IIS 1849359, CNS 1932482 and CCF 2029543.

REFERENCES

- Peter Armstrong, Alan G Wilson, Paul Dee, David M Hansell, et al. *Imaging of diseases of the chest.* Number Ed. 3. Mosby International 14d, 2000
- [2] Brian J Bartholmai, Sushravya Raghunath, Ronald A Karwoski, Teng Moua, Srinivasan Rajagopalan, Fabien Maldonado, Paul A Decker, and Richard A Robb. Quantitative ct imaging of interstitial lung diseases. *Journal of thoracic imaging*, 28(5), 2013.
- [3] Paulo Blikstein. Multimodal learning analytics. In Proceedings of the third international conference on learning analytics and knowledge, pages 102–106, 2013.
- [4] Lodewijk Brand, Kai Nichols, Hua Wang, Li Shen, and Heng Huang. Joint multi-modal longitudinal regression and classification for alzheimer's disease prediction. *IEEE Transactions on Medical Imaging*, 2019
- [5] Federico Cismondi, André S Fialho, Susana M Vieira, Shane R Reti, João MC Sousa, and Stan N Finkelstein. Missing data in medical databases: Impute, delete or classify? Artificial intelligence in medicine, 58(1):63–72, 2013.
- [6] Padideh Danaee, Reza Ghaeini, and David A Hendrix. A deep learning approach for cancer detection and relevant gene identification. In PACIFIC SYMPOSIUM ON BIOCOMPUTING 2017, pages 219–229. World Scientific, 2017.
- [7] Chris Ding and Jieping Ye. 2-dimensional singular value decomposition for 2d maps and images. In *Proceedings of the 2005 SIAM International Conference on Data Mining*, pages 32–43. SIAM, 2005.
- [8] Chris Ding, Ding Zhou, Xiaofeng He, and Hongyuan Zha. R 1-pca: rotational invariant 1 1-norm principal component analysis for robust subspace factorization. In *Proceedings of the 23rd international conference on Machine learning*, pages 281–288, 2006.
- [9] Garrett Fitzmaurice, Marie Davidian, Geert Verbeke, and Geert Molenberghs. *Longitudinal data analysis*. CRC press, 2008.

TABLE II

THE CLASSIFICATION PERFORMANCE OF THE LONGITUDINAL EMBEDDING AND ORIGINAL IMAGES WITH RESPECT TO GENDER DISTRIBUTION. SPECIFICALLY, WE COMPARED THE CLASSIFICATION RESULTS OF THE EMBEDDINGS AND THE ORIGINAL IMAGES USING THE F1 SCORE METRIC.

F1 Score	Gender	Ours	Dis-LSTM [10]	Ori-CNN [22]	2D-PCA [7]	R1-PCA [8]
Pneumonia	Male Female	$\begin{array}{c} 0.832 \pm 0.023 \\ 0.827 \pm 0.022 \end{array}$	$\begin{array}{c} 0.816 \pm 0.029 \\ 0.813 \pm 0.028 \end{array}$	$\begin{array}{c} 0.818 \pm 0.027 \\ 0.805 \pm 0.026 \end{array}$	$\begin{array}{c} 0.792\pm0.031 \\ 0.775\pm0.030 \end{array}$	$\begin{array}{c} 0.808 \pm 0.026 \\ 0.797 \pm 0.025 \end{array}$
Pneumothorax	Male Female	$\begin{array}{c} 0.830 \pm 0.024 \\ 0.824 \pm 0.023 \end{array}$	$\begin{array}{c} 0.819 \pm 0.030 \\ 0.807 \pm 0.029 \end{array}$	$\begin{array}{c} 0.821 \pm 0.028 \\ 0.809 \pm 0.027 \end{array}$	$\begin{array}{c} 0.805 \pm 0.032 \\ 0.799 \pm 0.031 \end{array}$	$\begin{array}{c} 0.808 \pm 0.027 \\ 0.805 \pm 0.026 \end{array}$
Edema	Male Female	$\begin{array}{c} 0.828 \pm 0.022 \\ 0.820 \pm 0.022 \end{array}$	$\begin{array}{c} 0.812\pm0.028 \\ 0.808\pm0.028 \end{array}$	$\begin{array}{c} 0.814 \pm 0.026 \\ 0.808 \pm 0.026 \end{array}$	$\begin{array}{c} 0.791 \pm 0.030 \\ 0.788 \pm 0.030 \end{array}$	$\begin{array}{c} 0.799 \pm 0.025 \\ 0.796 \pm 0.025 \end{array}$
Lung Lesion	Male Female	$\begin{array}{c} 0.810\pm0.021 \\ 0.802\pm0.021 \end{array}$	$\begin{array}{c} 0.796 \pm 0.027 \\ 0.782 \pm 0.027 \end{array}$	$\begin{array}{c} 0.796 \pm 0.025 \\ 0.783 \pm 0.025 \end{array}$	$\begin{array}{c} 0.776 \pm 0.029 \\ 0.769 \pm 0.029 \end{array}$	$\begin{array}{c} 0.791 \pm 0.024 \\ 0.777 \pm 0.024 \end{array}$
Lung Opacity	Male Female	$\begin{array}{c} 0.836 \pm 0.023 \\ 0.818 \pm 0.022 \end{array}$	$\begin{array}{c} 0.817 \pm 0.029 \\ 0.807 \pm 0.028 \end{array}$	$\begin{array}{c} 0.818 \pm 0.027 \\ 0.807 \pm 0.026 \end{array}$	$\begin{array}{c} 0.803 \pm 0.031 \\ 0.795 \pm 0.030 \end{array}$	$\begin{array}{c} 0.808 \pm 0.026 \\ 0.803 \pm 0.025 \end{array}$
F1 Score	Gender	L1-2DPCA [21]	AE [28]	LPP [13]	RBM [14]	Original
Pneumonia	Male Female	$\begin{array}{c} 0.812 \pm 0.030 \\ 0.794 \pm 0.029 \end{array}$	$\begin{array}{c} 0.818 \pm 0.025 \\ 0.815 \pm 0.024 \end{array}$	$\begin{array}{c} 0.814 \pm 0.028 \\ 0.799 \pm 0.027 \end{array}$	$\begin{array}{c} 0.793 \pm 0.032 \\ 0.780 \pm 0.031 \end{array}$	$\begin{array}{c} 0.781 \pm 0.024 \\ 0.764 \pm 0.023 \end{array}$
Pneumothorax	Male Female	$\begin{array}{c} 0.780 \pm 0.031 \\ 0.786 \pm 0.030 \end{array}$	$\begin{array}{c} 0.809 \pm 0.026 \\ 0.797 \pm 0.025 \end{array}$	$\begin{array}{c} 0.803 \pm 0.029 \\ 0.788 \pm 0.028 \end{array}$	$\begin{array}{c} 0.800 \pm 0.033 \\ 0.786 \pm 0.032 \end{array}$	$\begin{array}{c} 0.773 \pm 0.025 \\ 0.777 \pm 0.024 \end{array}$
Edema	Male Female	$\begin{array}{c} 0.789 \pm 0.029 \\ 0.769 \pm 0.029 \end{array}$	$\begin{array}{c} 0.809 \pm 0.024 \\ 0.802 \pm 0.024 \end{array}$	$\begin{array}{c} 0.804 \pm 0.027 \\ 0.795 \pm 0.027 \end{array}$	$\begin{array}{c} 0.809 \pm 0.031 \\ 0.807 \pm 0.031 \end{array}$	$\begin{array}{c} 0.766 \pm 0.023 \\ 0.761 \pm 0.023 \end{array}$
Lung Lesion	Male Female	$\begin{array}{c} 0.792 \pm 0.028 \\ 0.768 \pm 0.028 \end{array}$	$\begin{array}{c} 0.795 \pm 0.023 \\ 0.779 \pm 0.023 \end{array}$	$\begin{array}{c} 0.781 \pm 0.026 \\ 0.768 \pm 0.026 \end{array}$	0.776 ± 0.030 0.765 ± 0.030	$\begin{array}{c} 0.766 \pm 0.022 \\ 0.764 \pm 0.022 \end{array}$
Lung Opacity	Male Female	$\begin{array}{c} 0.788 \pm 0.030 \\ 0.792 \pm 0.029 \end{array}$	0.809 ± 0.025 0.804 ± 0.024	0.804 ± 0.028 0.786 ± 0.027	$\begin{array}{c} 0.781 \pm 0.032 \\ 0.774 \pm 0.031 \end{array}$	$\begin{array}{c} 0.771 \pm 0.024 \\ 0.764 \pm 0.023 \end{array}$

- [10] Riqiang Gao, Yuankai Huo, Shunxing Bao, Yucheng Tang, Sanja L Antic, Emily S Epstein, Aneri B Balar, Steve Deppen, Alexis B Paulson, Kim L Sandler, et al. Distanced lstm: time-distanced gates in long short-term memory models for lung cancer detection. In International Workshop on Machine Learning in Medical Imaging, pages 310-318. Springer, 2019.
- [11] Christian Garbin, Pranav Rajpurkar, Jeremy Irvin, Matthew P Lungren, and Oge Marques. Structured dataset documentation: a datasheet for chexpert. arXiv preprint arXiv:2105.03020, 2021.
- [12] ShuYi Gu, XiaoJun Deng, QingYun Li, XianWen Sun, JinFu Xu, and HuiPing Li. Gender differences of chronic obstructive pulmonary disease associated with manifestations on hrct. The clinical respiratory journal, 11(1):28-35, 2017.
- [13] Xiaofei He and Partha Niyogi. Locality preserving projections. Advances in neural information processing systems, 16:153-160, 2003.
- [14] Geoffrey E Hinton and Ruslan R Salakhutdinov. Reducing the dimensionality of data with neural networks. science, 313(5786):504-507,
- [15] Gao Huang, Zhuang Liu, Laurens Van Der Maaten, and Kilian Q Weinberger. Densely connected convolutional networks. In Proceedings of the IEEE conference on computer vision and pattern recognition, pages 4700-4708, 2017.
- [16] Jeremy Irvin, Pranav Rajpurkar, Michael Ko, Yifan Yu, Silviana Ciurea-Ilcus, Chris Chute, Henrik Marklund, Behzad Haghgoo, Robyn L. Ball, Katie S. Shpanskaya, Jayne Seekins, David A. Mong, Safwan S. Halabi, Jesse K. Sandberg, Ricky Jones, David B. Larson, Curtis P. Langlotz, Bhavik N. Patel, Matthew P. Lungren, and Andrew Y. Ng. Chexpert: A large chest radiograph dataset with uncertainty labels and expert comparison. CoRR, abs/1901.07031, 2019.
- [17] Rachna Jain, Meenu Gupta, Soham Taneja, and D Jude Hemanth. Deep learning based detection and analysis of covid-19 on chest x-ray images. Applied Intelligence, 51(3):1690-1700, 2021.
- [18] Mi-Jin Kang, Chang Min Park, Chang-Hyun Lee, Jin Mo Goo, and Hyun Ju Lee. Dual-energy ct: clinical applications in various pulmonary diseases. Radiographics, 30(3):685-698, 2010.
- [19] Konstantina Kourou, Themis P Exarchos, Konstantinos P Exarchos, Michalis V Karamouzis, and Dimitrios I Fotiadis. Machine learning

- applications in cancer prognosis and prediction. Computational and structural biotechnology journal, 13:8-17, 2015.
- [20] Philippe Lambin, Ruud GPM Van Stiphout, Maud HW Starmans, Emmanuel Rios-Velazquez, Georgi Nalbantov, Hugo JWL Aerts, Erik Roelofs, Wouter Van Elmpt, Paul C Boutros, Pierluigi Granone, et al. Predicting outcomes in radiation oncology-multifactorial decision support systems. Nature reviews Clinical oncology, 10(1):27-40, 2013.
- [21] Xuelong Li, Yanwei Pang, and Yuan Yuan. L1-norm-based 2dpca. IEEE Transactions on Systems, Man, and Cybernetics, Part B (Cybernetics), 40(4):1170-1175, 2010.
- [22] Fangzhou Liao, Ming Liang, Zhe Li, Xiaolin Hu, and Sen Song. Evaluate the malignancy of pulmonary nodules using the 3-d deep leaky noisy-or network. IEEE transactions on neural networks and learning systems, 30(11):3484-3495, 2019.
- [23] Lyujian Lu, Saad Elbeleidy, Lauren Baker, Hua Wang, Li Shen, and Huang Heng. Improved prediction of cognitive outcomes via globally aligned imaging biomarker enrichments over progressions. IEEE Transactions on Biomedical Engineering, 68(11):3336-3346, 2021.
- [24] Lyujian Lu, Hua Wang, Saad Elbeleidy, and Feiping Nie. Predicting cognitive declines using longitudinally enriched representations for imaging biomarkers. In Proceedings of the IEEE/CVF Conference on Computer Vision and Pattern Recognition, pages 4827-4836, 2020.
- [25] Feiping Nie, Hua Wang, Heng Huang, and Chris Ding. Adaptive loss minimization for semi-supervised elastic embedding. In Twenty-Third International Joint Conference on Artificial Intelligence, 2013.
- [26] Pranav Rajpurkar, Jeremy Irvin, Kaylie Zhu, Brandon Yang, Hershel Mehta, Tony Duan, D Ding, Aarti Bagul, C Langlotz, K Shpanskaya, et al. Radiologist-level pneumonia detection on chest x-rays with deep learning. arXiv preprint arXiv:1711.05225, 2017.
- [27] Shine Raju, Subha Ghosh, and Atul C Mehta. Chest ct signs in
- pulmonary disease: a pictorial review. *Chest*, 151(6):1356–1374, 2017. [28] Pascal Vincent, Hugo Larochelle, Isabelle Lajoie, Yoshua Bengio, Pierre-Antoine Manzagol, and Léon Bottou. Stacked denoising autoencoders: Learning useful representations in a deep network with a local denoising criterion. Journal of machine learning research, 11(12), 2010.
- [29] Hua Wang, Feiping Nie, and Heng Huang. Multi-view clustering and feature learning via structured sparsity. In International conference on machine learning, pages 352-360, 2013.